CellPress

Cancer Cell
Article

MTDH-SND1 Interaction Is Crucial for Expansion and Activity of Tumor-Initiating Cells in Diverse Oncogene- and Carcinogen-Induced Mammary Tumors

Liling Wan,[1] Xin Lu,[1,6] Salina Yuan,[1] Yong Wei,[1] Feng Guo,[2] Minhong Shen,[1] Min Yuan,[1] Rumela Chakrabarti,[1] Yuling Hua,[1] Heath A. Smith,[1] Mario Andres Blanco,[1,7] Marina Chekmareva,[3] Hao Wu,[4] Roderick T. Bronson,[5] Bruce G. Haffty,[4] Yongna Xing,[2] and Yibin Kang[1,4,*]

[1]Department of Molecular Biology, Princeton University, Princeton, NJ 08544, USA
[2]McArdle Laboratory, Department of Oncology, University of Wisconsin-Madison, School of Medicine and Public Health, Madison, WI 53706, USA
[3]Pathology and Laboratory Medicine, Robert Wood Johnson Medical School, Rutgers University, Piscataway, NJ 08903, USA
[4]Rutgers Cancer Institute of New Jersey, New Brunswick, NJ 08903, USA
[5]Department of Pathology, Harvard Medical School, Boston, MA 02115, USA
[6]Present address: Departments of Cancer Biology, Genomic Medicine, and Experimental Radiation Oncology and Institute of Applied Cancer Science, University of Texas MD Anderson Cancer Center, Houston, TX 77030, USA
[7]Present address: Department of Cell Biology, Harvard Medical School, Boston, MA 02115, USA
*Correspondence: ykang@princeton.edu
http://dx.doi.org/10.1016/j.ccr.2014.04.027

SUMMARY

The Metadherin gene (*MTDH*) is prevalently amplified in breast cancer and associated with poor prognosis; however, its functional contribution to tumorigenesis is poorly understood. Using mouse models representing different subtypes of breast cancer, we demonstrated that MTDH plays a critical role in mammary tumorigenesis by regulating oncogene-induced expansion and activities of tumor-initiating cells (TICs), whereas it is largely dispensable for normal development. Mechanistically, MTDH supports the survival of mammary epithelial cells under oncogenic/stress conditions by interacting with and stabilizing *Staphylococcal* nuclease domain-containing 1 (SND1). Silencing MTDH or SND1 individually or disrupting their interaction compromises tumorigenenic potential of TICs in vivo. This functional significance of MTDH-SND1 interaction is further supported by clinical analysis of human breast cancer samples.

INTRODUCTION

Cancer is characterized by rampant genetic and epigenetic alterations. Recurrent DNA copy number alterations often indicate the presence of key drivers of cancer at the affected loci. We previously identified Metadherin (*MTDH;* also called *AEG1*, *LYRIC*) as a prometastasis gene that resides in 8q22, a frequently amplified genomic locus linked to poor relapse-free survival of breast cancer (Hu et al., 2009). Notably, overexpression of MTDH is observed in more than 40% of primary breast tumors and is an independent factor for poor prognosis (Hu et al., 2009). What drives the strong selection of MTDH in primary breast tumors is unclear and the functional significance of MTDH in normal development and tumorigenesis remains poorly understood.

Recent studies using cell culture or xenograft models have implicated MTDH in several cancer-related processes, including proliferation, cell death, invasion, and angiogenesis (Emdad et al., 2013), although the underlying mechanistic understanding of MTDH in these processes remains limited to date. In breast cancer, MTDH was postulated to be a transmembrane protein that mediates the adhesion of cancer cells to the lung endothelium (Brown and Ruoslahti, 2004). In certain cancer types, MTDH

Significance

Our finding that MTDH is required for the expansion and function of both luminal and basal breast TICs underscores the selection pressure to overexpress MTDH in diverse breast tumor subtypes. We also show that MTDH is crucial for TICs but not mammary stem cells, suggesting that it is different from many cell fate determinants that regulate both normal and cancerous stem cells. The functional dependency of MTDH on its conserved interaction with SND1, together with the observation that systemic deletion of MTDH is well tolerated in mice, suggest that targeting the MTDH-SND1 complex may offer an opportunity to control tumor initiation, recurrence, and metastasis by preventing the expansion of TICs, with minimal impact on normal tissues.

has been linked to multiple oncogenic pathways such as phosphoinositide 3-kinase/protein kinase B and nuclear factor κ-light-chain-enhancer of activated B cells (Emdad et al., 2013). However, how MTDH regulates these pathways remains elusive. Although evolutionarily conserved in higher vertebrates, MTDH contains no recognizable functional domain, rendering the understanding of its biological function challenging. Multiple groups have identified several MTDH-binding partners, including promyelocytic leukemia zinc finger, BCCIPα, and *Staphylococcal* nuclease domain-containing 1 (SND1; Wan and Kang, 2013). However, whether and how the interactions with these proteins mediate the function of MTDH is largely unknown.

Breast cancer is a heterogeneous disease that can be broadly classified into luminal and basal-like subtypes based on gene expression profiles (Perou et al., 2000). It has been speculated that different oncogenic signaling may target different cells of origin, thus leading to the formation of different subtypes of breast cancer. However, the origin, identity, and regulation of tumor-initiating cells (TICs) in different oncogene-induced mammary tumors remain poorly characterized. Autochthonous tumorigenesis in mice offers great models for tracking the early changes during tumor initiation and for investigating the role of a gene of interest in mediating the transformation and expansion of TICs. In this study, we investigate the function of MTDH in breast cancer initiation and progression.

RESULTS

Mtdh-Knockout Mice Were Viable and Grossly Indistinguishable from Wild-Type Mice

To generate *Mtdh*-knockout (KO) mice, we screened the Bay Genomics gene trap database and selected ESC line XB780, which contains an insertion into the second intron of *Mtdh* that results in premature termination of transcription (Figure 1A). Injection of XB780 ES cells into blastocysts generated chimeric mice with subsequent confirmation of germline transmission (Figure S1A available online). Crosses between *Mtdh* heterozygous ($Mtdh^{+/-}$) mice gave rise to offspring at the Mendelian ratio. *Mtdh* homozygous KO ($Mtdh^{-/-}$) embryos showed widespread LacZ activity (Figure 1B), suggesting ubiquitous *Mtdh* expression in many embryonic organs. In adult mice, MTDH was also detected in a variety of tissues in wild-type (WT, $Mtdh^{+/+}$) and $Mtdh^{+/-}$ mice, while undetectable in $Mtdh^{-/-}$ mice (Figure S1B), confirming that the gene-trapped allele completely abolished *Mtdh* expression. $Mtdh^{-/-}$ mice were viable, fertile, and displayed no obvious abnormalities when monitored for up to 2 years (data not shown).

MTDH was also detected in normal mammary epithelial cells (MECs) and the expression levels correlated with *Mtdh* genetic status (Figure 1C). To assess the influence of MTDH deficiency in postnatal mammary gland development, whole mounts of inguinal mammary fat pads from WT and KO virgin mice were examined (Figure S1C). Except for a transient delay in ductal outgrowth of mammary glands from 3- and 5-week-old KO mice as compared to WT littermates, we did not observe significant differences in branching morphogenesis at later time points (Figure S1D) or during pregnancy and lactation (Figures S1E and S1F). The largely comparable mammary epithelium in WT and $Mtdh^{-/-}$ mice starting at puberty therefore allows us to use $Mtdh^{-/-}$ mice to examine the necessity of MTDH for mammary tumor formation.

Mtdh KO Inhibits the Formation and Metastasis of Luminal Mammary Tumors

To dissect the roles of MTDH during autochthonous mammary tumor progression, we first used the MMTV-PyMT and MMTV-ErbB2 transgenic models, both of which develop luminal adenocarcinoma with a high incidence of lung metastasis. In the aggressive MMTV-PyMT model, mammary tumors occurred as early as 42 days of age, and by day 63, 50% of $Mtdh^{+/+}$ mice developed tumors (Figure 1D). In contrast, the first palpable tumor was detected in the $Mtdh^{-/-}$ group at day 50, and 50% of these mice developed tumors only after 80 days. The delay in tumor occurrence was further supported by a greater number of tumor-free mammary glands in $Mtdh^{-/-}$ mice as compared to WT control (Figure 1E). Consistently, the total tumor burden of *PyMT*;$Mtdh^{+/-}$ and *PyMT*;$Mtdh^{-/-}$ mice was reduced to 54% and 10% of that of WT control, respectively (Figure 1F). Furthermore, *PyMT*;$Mtdh^{-/-}$ mice had significantly fewer (Figure 1G) and smaller ($p < 0.05$, data not shown) metastatic nodules.

The difference in tumor formation was even more prominent in the MMTV-ErbB2 model, in which tumorigenesis occurs after long latency. Whereas almost all *ErbB2*;$Mtdh^{+/+}$ mice developed tumors by 300 days of age, more than 60% of *ErbB2*;$Mtdh^{-/-}$ mice had no tumors (Figures 1H and 1I). Even when monitored for up to 18 months, 30% of *ErbB2*;$Mtdh^{-/-}$ mice ($n = 68$) still remained completely tumor-free, whereas all *ErbB2*;$Mtdh^{+/+}$ mice ($n = 61$) had either died or reached the morbidity criteria for euthanization ($p < 0.0001$). Lung metastasis was also severely impaired in *ErbB2*;$Mtdh^{-/-}$ mice (Figures 1J and 1K).

The difference in mammary tumor formation was not due to the differential induction of oncogenes because the expression of PyMT (Figure S1G) and ErbB2 (Figures S1H and S1I) was comparable between WT and KO mammary glands or tumors. In addition, the activation of ErbB2, as indicated by its phosphorylation, was not affected (Figures S1H and S1I). Furthermore, MTDH protein levels were elevated in PyMT- and ErbB2-driven tumors as compared to age-matched normal controls (Figures S1J and S1K), suggesting that high levels of MTDH may confer growth advantage to MECs during tumorigenesis.

Mtdh KO Restrains the Formation of Basal-like and Mixed Subtypes of Mammary Tumors

We further expanded our investigation of MTDH in tumor formation to the MMTV-Wnt model, which develops tumors that exhibit mammary stem cell (MaSC)-like gene expression profiles and resemble the basal subtype of human breast cancer (Herschkowitz et al., 2007). While virtually all *Wnt;*$Mtdh^{+/+}$ mice succumbed to cancer at 300 days of age, no tumors were detected in 35% of *Wnt;*$Mtdh^{+/-}$ and 62% of *Wnt;*$Mtdh^{-/-}$ mice (Figure 1L). The multiplicity of tumors was also highly dependent on the gene dosage of *Mtdh* (Figure 1M). These phenotypes markedly resembled what we observed in the luminal tumor models. To broaden our analysis, we induced mammary carcinogenesis using combined treatment of medroxyprogesterone acetate (MPA) and 7, 12-dimethylbenzanthracene (DMBA) (Figure 1N), which resulted in the formation of mammary tumors with histological characteristics of adenocarcinoma,

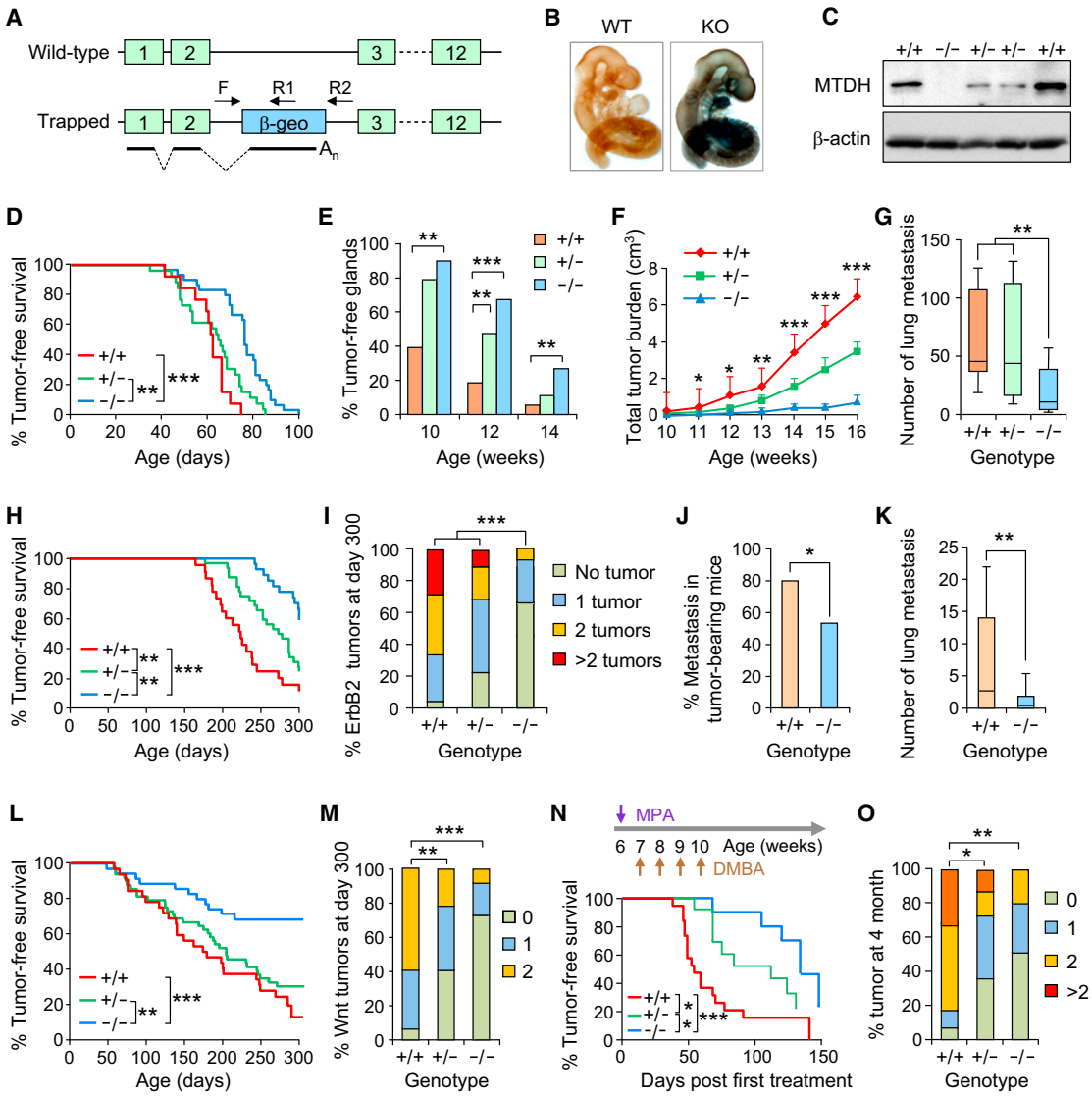

Figure 1. Systemic Deletion of *Mtdh* Inhibits Mammary Tumor Formation and Metastasis

(A) Schematic representation of WT and mutant *Mtdh* allele. Green boxes represent exons 1–12. Primers (F, forward; R, reverse) used for genotyping are indicated above the corresponding genomic sequences.

(B) LacZ expression in WT and KO embryo at day 10.5, depicted with X-gal staining.

(C) MTDH protein immunobloting in MECs freshly dissociated from 8-week-old female mice with indicated *Mtdh* genotype.

(D) Kinetics of mammary tumor onset in MMTV-PyMT females of indicated *Mtdh* genotypes. $Mtdh^{+/+}$ (n = 13), $Mtdh^{+/-}$ (n = 26), and $Mtdh^{-/-}$ (n = 30).

(E) Percentage of tumor-free mammary glands at indicated ages in the same cohort of mice as in (D).

(F) Total tumor burden of *PyMT;*$Mtdh^{+/+}$, *PyMT;*$Mtdh^{+/-}$, and *PyMT;*$Mtdh^{-/-}$ cohorts evaluated at indicated age. Statistical comparison was done between $Mtdh^{+/+}$ and $Mtdh^{-/-}$ *groups*. Data represent mean ± SEM (n > 20).

(G) Number of lung metastatic nodules in *PyMT;*$Mtdh^{+/+}$ (n = 15), *PyMT;*$Mtdh^{+/-}$ (n = 11), and *PyMT;*$Mtdh^{-/-}$ (n = 14) animals. Error bars represent the 5th to 95th percentiles.

(H) Kinetics of mammary tumor onset in MMTV-ErbB2 mice of the indicated genotypes. $Mtdh^{+/+}$ (n = 22), $Mtdh^{+/-}$ (n = 31), and $Mtdh^{-/-}$ (n = 27).

(I) Percentage of mice from same cohorts as in (H) bearing indicated number of tumors at 300 days of age.

(J) Incidence of lung metastasis in tumor-bearing MMTV-ErbB2 mice from $Mtdh^{+/+}$ (n = 30) and $Mtdh^{-/-}$ (n = 23) groups.

(K) Number of metastatic lesions per lung section in the same cohorts of mice from (J). Error bars represent the 5th to 95th percentiles.

(L) Kinetics of mammary tumor onset in MMTV-Wnt mice of the indicated genotypes. $Mtdh^{+/+}$ (n = 31), $Mtdh^{+/-}$ (n = 48), and $Mtdh^{-/-}$ (n = 31).

(M) Percentage of mice from same cohorts as in (L) bearing indicated number of tumors at 300 days of age.

(N) Kinetics of mammary tumor onset in mice with indicated *Mtdh* genotype treated with MPA and DMBA as indicated (top). Tumor latency was recorded as days after first DMBA treatment. $Mtdh^{+/+}$ (n = 19), $Mtdh^{+/-}$ (n = 13), and $Mtdh^{-/-}$ (n = 10).

(O) Percentage of mice from same cohorts as in (N) bearing indicated number of tumors at 4 months of age.

Statistics: (D, H, L, and N) log rank test. (E, I, J, M, and O) Chi-square test. (G and K) Mann-Whitney test. (F) Student's t test. ***p < 0.001, **p < 0.01, *p < 0.05. See also Figure S1.

adenosquamous carcinoma and adenomyoepithelioma carcinoma (Yin et al., 2005). Again, *Mtdh*$^{-/-}$ females showed markedly attenuated tumor susceptibility after MPA/DMBA treatment (Figures 1N and 1O).

Mtdh KO Impairs the Expansion and Activities of Oncogene-Induced Basal and Luminal TICs

The dramatic effect of *Mtdh* deletion on mammary tumor formation prompted us to investigate early events during tumorigenesis. To this end, we examined whole mounts (Figure 2A, top) and hematoxylin and eosin-stained sections (Figure 2A, bottom) of mammary glands from different tumor models at preneoplastic stages. Both the *PyMT* and *Wnt* oncogenes induced extensive hyperplasia as early as 4 weeks in *Mtdh*$^{+/+}$ mice; however, *Mtdh*$^{-/-}$ glands exhibited significantly fewer and smaller hyperplasia foci mingled with normal ductal structures. MMTV-ErbB2 mice have the longest tumor latency, and this corresponds to significantly delayed and the least severe hyperplasia. Whole mount analysis of mammary glands from 6-month-old tumor-free MMTV-ErbB2 females revealed close to 100% incidence of hyperplasia in *Mtdh*-positive mice, whereas only 20% of those from *ErbB2;Mtdh*$^{-/-}$ mice were mildly hyperplasic (Figures S2A and S2B).

These severely impaired preneoplastic changes in *Mtdh*$^{-/-}$ glands may suggest a defect in the expansion of transformed MECs. To examine oncogene-induced changes in the cellular composition of mammary glands, we profiled preneoplastic mammary glands using CD24, CD29 (β1 integrin) and CD61 (β3 integrin), which have been previously used to resolve luminal and basal mammary epithelial subsets (Asselin-Labat et al., 2007; Shackleton et al., 2006). Compared to normal glands, PyMT preneoplastic tissues displayed a drastic expansion of the Lin$^-$CD24$^+$CD29^{low} luminal subset (CD24$^+$CD29^{low}; Figures 2B and 2C), consistent with previous reports of "luminal-like" gene expression profiles (Herschkowitz et al., 2007). In contrast, the percentage of Lin$^-$CD24$^+$CD29^{high} (CD24$^+$CD29^{hi}) basal population, which enriches for MaSCs, was markedly increased in preneoplastic tissues from Wnt mammary glands (Figures 2B and 2D), as previously noted (Shackleton et al., 2006), suggesting that this population represents a key cell target for transformation in this model. Intriguingly, these oncogene-specific perturbations of the epithelial hierarchy were compromised by *Mtdh* loss, as evidenced by (1) the lack of CD24$^+$CD29^{low} luminal subset expansion in *PyMT;Mtdh*$^{-/-}$glands (Figures 2B and 2C), and (2) a significant decrease in the expansion of the CD24$^+$CD29^{hi} basal subset in *Wnt;Mtdh*$^{-/-}$ glands (Figures 2B and 2D) compared to WT counterparts. PyMT- or Wnt-induced hyperplastic glands in *Mtdh*$^{+/+}$ mice did not exhibit a selective expansion of CD61$^+$ population as compared to normal glands (Figures S2C and S2D, compare orange bars). However, we noticed that the percentage of CD61$^+$ cells, which were more capable of forming mammospheres than CD61$^-$ cells (Figure S2E), was significantly decreased in *Wnt;Mtdh*$^{-/-}$ glands as compared to *Wnt;Mtdh*$^{+/+}$ glands (Figures S2C and S2D, compare WT versus KO).

To test whether *Mtdh*$^{-/-}$ preneoplastic glands indeed contain fewer TICs, we dissociated primary MECs (pMECs) from *Mtdh*$^{+/+}$ and *Mtdh*$^{-/-}$ preneoplastic glands and performed in vitro mammosphere formation assays. *Mtdh*$^{-/-}$ pMECs formed a decreased number of spheres across multiple tumor models (Figure 2E). Moreover, when orthotopically transplanted into WT recipient mice, *PyMT;Mtdh*$^{-/-}$ pMECs contained substantially fewer tumor-repopulating cells in vivo as revealed by reduced tumor incidence when a series of diluting numbers were tested (Figure 2F).

We further asked whether PyMT-induced TICs exist in the expanded luminal population. Sorted luminal and basal pMECs from preneoplastic glands of *PyMT* mice were transplanted in vivo. Tumors were detected at high frequency in mice that received luminal but not basal cells (Figure 2G), suggesting PyMT-induced preneoplastic TICs were copurified with luminal subset of MECs. Importantly, when the tumorigenic capabilities of luminal cells from *PyMT;Mtdh*$^{+/+}$ and *PyMT;Mtdh*$^{-/-}$ females were examined in vivo, tumor incidence (Figure 2H) and volumes (Figure 2I) were substantially decreased in mice transplanted with *Mtdh*$^{-/-}$ cells. These results suggest that not only the expansion, but also the tumorigenic potential of luminal cells is severely compromised in *PyMT;Mtdh*$^{-/-}$ mice.

We did not detect a selective expansion of either luminal or basal subset of MECs in MMTV-ErbB2 preneoplastic glands as compared to normal control (data not shown), in accordance with a previous report (Shackleton et al., 2006). To identify which subset of MECs serves as TICs, we sorted out luminal and basal MECs from *ErbB2;Mtdh*$^{+/+}$ hyperplastic glands and orthotopically transplanted these cells. Palpable tumors were detected in 100% of the mice that received either luminal or basal MECs (Figures S2F and S2G). Regardless of cell origin, all tumors closely resembled spontaneous tumors from MMTV-ErbB2 mice in histology (Figure S2H). These results suggest MMTV-ErbB2 tumors may originate from both luminal and basal compartments, and basal cells can give rise to luminal type of tumors, a finding supported by a recent report (Zhang et al., 2013a). To identify the cellular targets that are dependent on MTDH, we also transplanted luminal and basal subsets from *ErbB2;Mtdh*$^{-/-}$ females in vivo. Strikingly, neither luminal nor basal *ErbB2;Mtdh*$^{-/-}$ cells gave rise to palpable tumors at the time when all the mice receiving *ErbB2;Mtdh*$^{+/+}$ cells had developed large tumors (Figures S2F and S2G). These results indicate that MTDH is critical for maintaining ErbB2-induced basal and luminal TICs.

In contrast to its essential role in regulating TICs at early tumorigenesis, MTDH is largely dispensable for adult MaSCs activities, as indicated by similar in vivo mammary gland reconstitution (Figure S2I) efficiency of either unfractionated Lin$^-$ MECs (Figure S2J) or MaSCs-enriched basal cells (Figures S2K and S2L) from WT and KO mice.

MEC-Intrinsic Role of MTDH in Promoting Mammary Tumor-Initiating Capacities

Because MTDH is widely expressed in mice (Figures 1B and S1B), the tumorigenesis defects in whole-organism KO mice could result from either loss of MTDH in MECs or other cell/tissue types. To distinguish between these two possibilities, we sought to re-introduce mouse MTDH specifically in MECs of *Mtdh*$^{-/-}$ mice in vivo and test whether this would rescue the tumorigenic defects. To this end, we created a MMTV-Mtdh transgenic mouse line (Figures 3A, S3A, and S3B) and observed expression of the *Mtdh* transgene specifically in the mammary gland, and, to

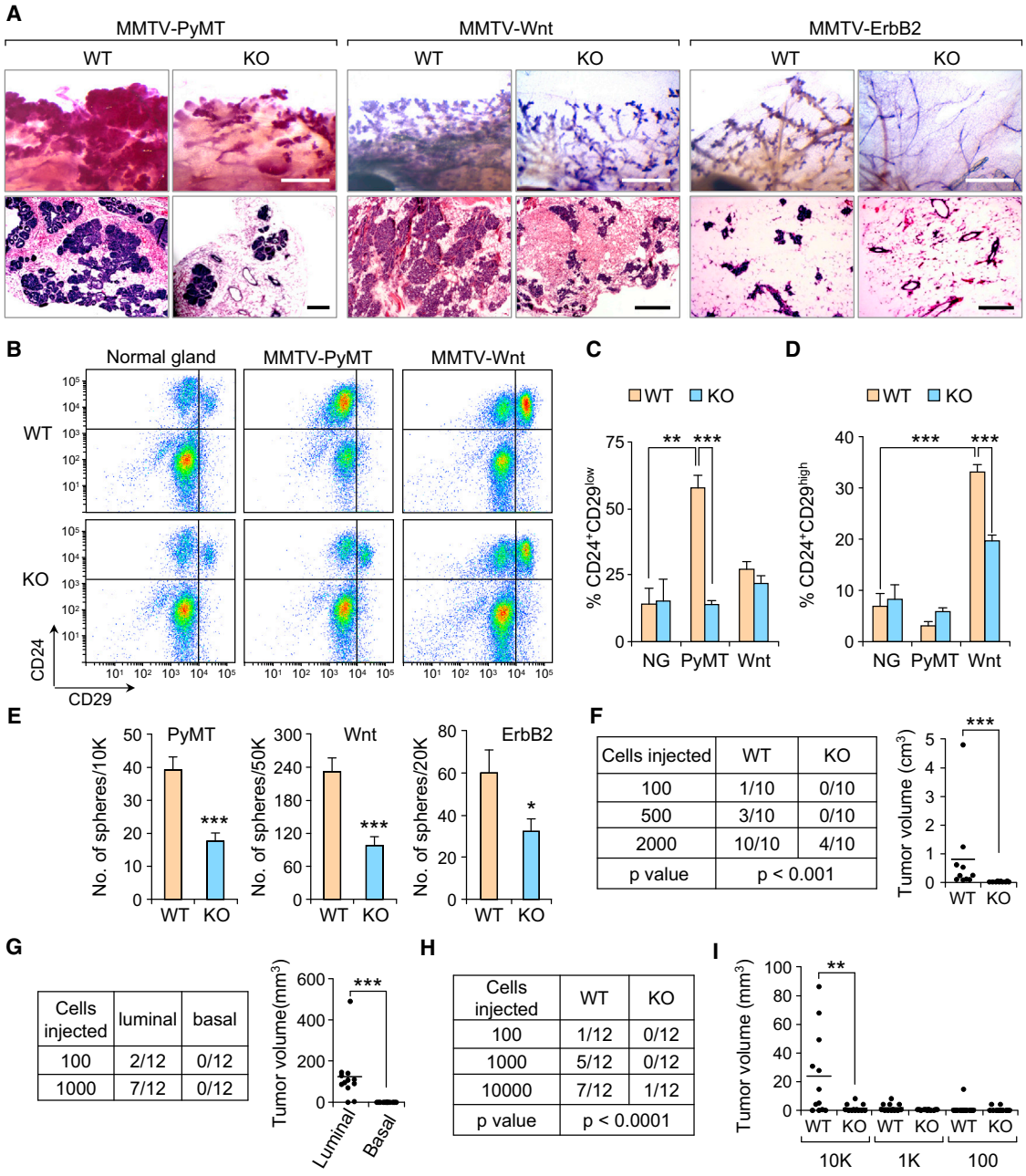

Figure 2. Mammary Glands from *Mtdh*$^{-/-}$ Mice Exhibit Defects in Oncogene-Induced Expansion and Tumorigenic Potential

(A) Representative whole mounts (top; scale bar represents 1 mm) and hematoxylin and eosin-stained sections (bottom; scale bar represents 200 μm) of preneoplastic mammary glands from MMTV-PyMT (4 weeks), MMTV-Wnt (6 weeks), and MMTV-ErbB2 (6 months) mice of the indicated genotypes.

(B) Flow cytometry of CD45$^-$CD31$^-$TER119$^-$ (Lin$^-$) MECs from mammary glands of 6-week-old females of the indicated genotypes.

(C and D) Quantification of luminal (C) and basal (D) cells analyzed in (B; n = 4).

(E) Mammosphere formation assays with WT or KO MECs dissociated from preneoplastic glands of MMTV-PyMT (n = 6), MMTV-Wnt (n = 4), and MMTV-ErbB2 (n = 6) mice. Assays performed in triplicate for each mammary gland.

(F) Mammary tumor incidence (left) and size (right) 3 months after orthotopic transplantations of unsorted MECs dissociated from preneoplastic glands of *PyMT;Mtdh*$^{+/+}$ and *PyMT;Mtdh*$^{-/-}$ mice.

(G) Mammary tumor incidence (left) and size (right) 8 weeks after orthotopic transplantations of indicated sorted CD24$^+$CD29^{low} luminal or CD24$^+$CD29^{high} basal MECs from preneoplastic glands of *PyMT;Mtdh*$^{+/+}$ mice.

(H and I) Mammary tumor incidence (H) and volumes (I) 8 weeks after orthotopic transplantations of Lin$^-$CD24$^+$CD29^{low} luminal cells from preneoplastic glands of *PyMT;Mtdh*$^{+/+}$ and *PyMT;Mtdh*$^{-/-}$ mice.

Statistics: (C–E) Student's t test. (F–I), tumor incidence based on limiting dilution analysis and tumor volume based on Mann-Whitney test. ***p < 0.001, **p < 0.01, *p < 0.05. Data represent mean ± SEM. See also Figure S2.

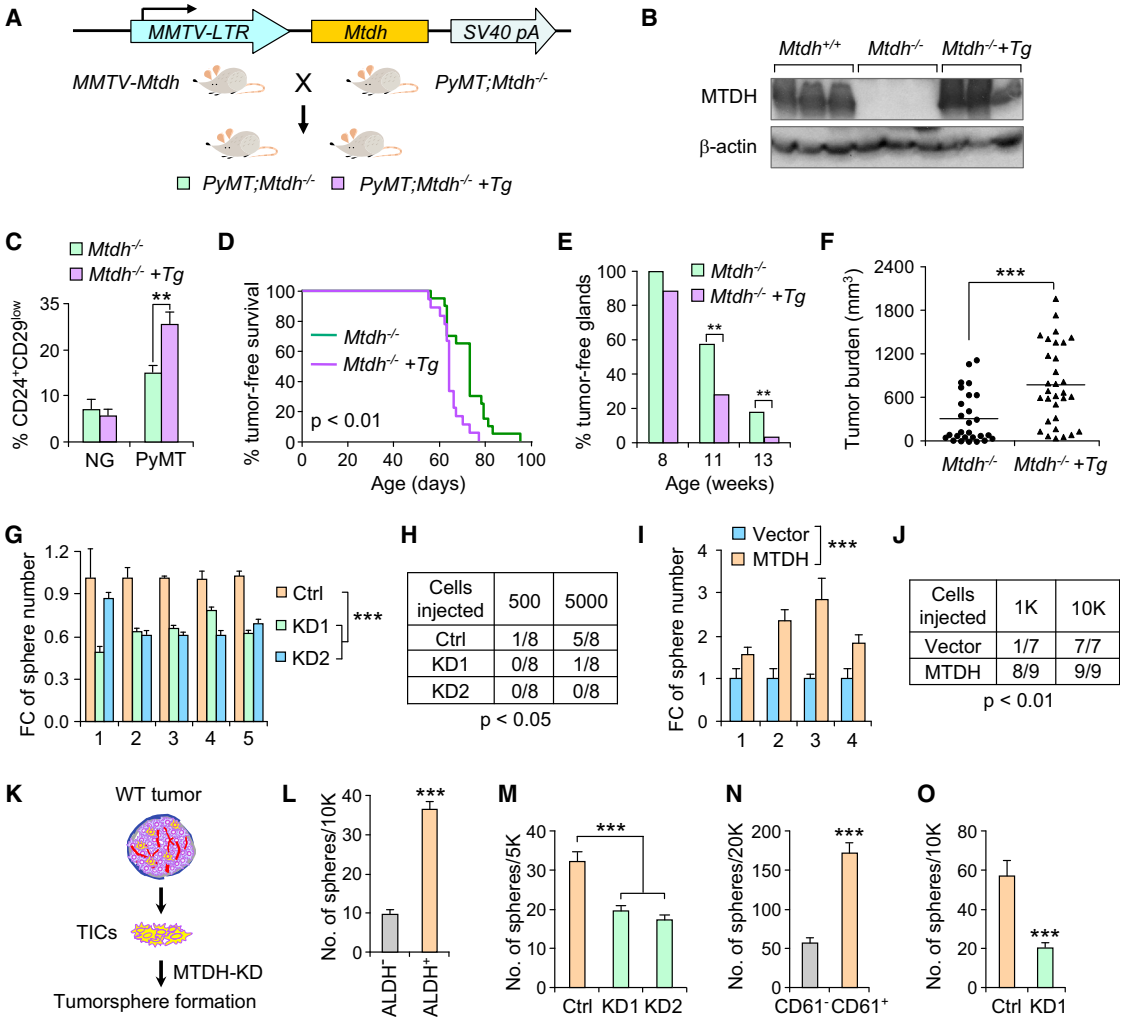

Figure 3. MTDH Is Intrinsically Required for Oncogene-Induced TICs Functionality

(A) Schematic diagram of *MMTV-Mtdh* transgene construct and breeding scheme used to generate *PyMT;Mtdh*$^{-/-}$ mice with (*Mtdh*$^{-/-}$ +*Tg*) or without the *MMTV-Mtdh* transgene.

(B) MTDH protein levels in PyMT-induced tumors from *Mtdh*$^{+/+}$, *Mtdh*$^{-/-}$, or *Mtdh*$^{-/-}$ +*Tg* mice.

(C) Quantification of CD24^{+}CD29^{low} luminal population in Lin^{-} MECs (n = 4) from preneoplastic mammary glands of 6-week-old females of the indicated genotypes.

(D) Kinetics of mammary tumor onset in MMTV-PyMT females of the indicated genotypes. *Mtdh*$^{-/-}$ (n = 21), *Mtdh*$^{-/-}$ +*Tg* (n = 20).

(E) Average number of tumor-free mammary glands at indicated ages in the same cohort of mice as in (D).

(F) Tumor burden of same cohorts of mice as in (D).

(G and H) MTDH was knocked down by two independent shRNA (KD1 and KD2) in freshly dissociated *PyMT;Mtdh*$^{+/+}$ pMECs and in vitro mammosphere (G; n = 5, each in triplicate) and in vivo tumor formation assays were performed (H; incidence at 3 months). FC, fold changes.

(I and J) Mouse MTDH was expressed in freshly dissociated *PyMT;Mtdh*$^{-/-}$ pMECs via lentivirus transduction and in vitro mammosphere (I; n = 4, each in triplicates) and in vivo tumor formation (J) assays were performed.

(K) Schematic diagram of experiments in (L–O).

(L) Mammosphere formation of ALDH^{+} or ALDH^{-} tumor cells from *PyMT;Mtdh*$^{+/+}$ tumors.

(M) MTDH was knocked down in sorted ALDH^{+} cells from *PyMT;Mtdh*$^{+/+}$ tumors and mammosphere assays were performed.

(N) Mammosphere formation of Lin^{-}CD24^{+}CD61^{+} or Lin^{-}CD24^{+}CD61^{-} tumor cells from *Wnt;Mtdh*$^{+/+}$ tumors.

(O) MTDH was knocked down in sorted Lin^{-}CD24^{+}CD61^{+} cells from *Wnt;Mtdh*$^{+/+}$ tumors and mammosphere assays were performed.

Statistics: (C, G, I, and L–O) Student's t test. (D) Log rank test. (E) Chi-square test. (F) Mann-Whitney test. (H and J) Limiting dilution analysis. ***p < 0.001, **p < 0.01, *p < 0.05. Data represent mean ± SEM. See also Figure S3.

a lesser extent, the salivary gland (Figure S3C). Next, we crossed these MMTV-Mtdh mice with *PyMT;Mtdh*$^{-/-}$ mice to generate *PyMT;Mtdh*$^{-/-}$ mice with or without exogenous *Mtdh* transgene (Figure 3A). Notably, transgene (*Tg*)-rescued *PyMT;Mtdh*$^{-/-}$ tumors expressed similar levels of MTDH as that of *PyMT;Mtdh*$^{+/+}$ tumors (Figure 3B). We observed a nearly 2-fold increase in the expansion of luminal cells from *PyMT;Mtdh*$^{-/-}$ +*Tg* preneoplastic glands as compared to *PyMT;Mtdh*$^{-/-}$ mice (Figure 3C).

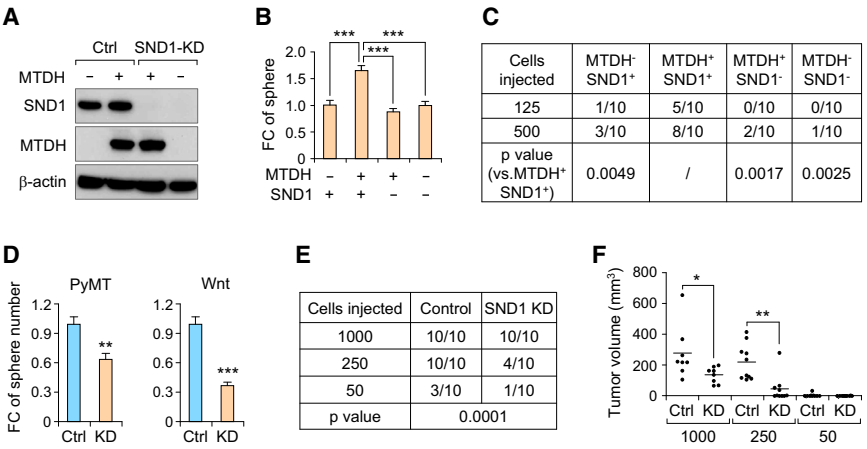

Figure 4. SND1 Is Necessary for MTDH-Mediated Tumor Initiation

(A) Combination of MTDH re-expression and SND1 knockdown in *PyMT;Mtdh*$^{-/-}$ tumor cells. The efficiency of SND1 KD and MTDH re-expression was assessed with western blotting.

(B and C) In vitro mammosphere (B) and in vivo tumor formation (C; 6 weeks) assays were performed with cells generated in (A). +/− indicate whether the denoted protein is present (+) or absent (−) based on western blotting results in (A).

(D) SND1 was knocked down in *PyMT;Mtdh*$^{+/+}$ or *Wnt;Mtdh*$^{+/+}$ pMECs cells and mammosphere assays were performed in triplicates.

(E and F) Tumor incidence (E) and volume (F) after orthotopic transplantations of control or SND1-KD *PyMT;Mtdh*$^{+/+}$ pMECs.

Statistics: (B and D) Student's t test. (C and E) Limiting dilution analysis. (F) Mann-Whitney test. ***$p < 0.001$, **$p < 0.01$, *$p < 0.05$. Data represent mean ± SEM. See also Figure S4.

In addition, tumor onset was accelerated (Figure 3D) and tumor incidence and burden (Figures 3E and 3F) was increased in the *PyMT;Mtdh*$^{-/-}$ +*Tg* group. Of note, the presence of the *Mtdh* transgene did not alter the histology of the resulting tumors (Figure S3D). These results strongly support a tumor-intrinsic role of MTDH in promoting target cell expansion and subsequent mammary tumorigenesis in vivo, although we cannot completely rule out the contribution of the tumor stroma.

To complement our spontaneous tumor model studies, we next investigated whether acute manipulation of MTDH also affects the tumorigeneic potential of preneoplastic MECs. We knocked down MTDH in pMECs freshly dissociated from preneoplastic glands of *PyMT;Mtdh*$^{+/+}$ (Figure 3G) and *ErbB2;Mtdh*$^{+/+}$ (Figure S3E) females. The sphere-forming capability of MTDH-knockdown (KD) cells was significantly reduced in multiple independent samples in both models (Figures 3G and S3E). In vivo tumor formation of *PyMT;Mtdh*$^{+/+}$ pMECs was also severely impaired by MTDH KD (Figure 3H). Conversely, when MTDH was restored in PyMT;*Mtdh*$^{-/-}$ pMECs via lentivirus transduction to a level that was comparable to WT counterparts (data not shown), both in vitro sphere and in vivo tumor formation were significantly enhanced (Figures 3I, 3J, and S3F–S3H).

We further asked whether TICs from established MTDH-positive tumors rely on MTDH for their functionality (Figure 3K). The fact that established tumors from PyMT, Wnt, and ErbB2-driven tumor models displayed one relatively homogenous population when profiled with CD24 and CD29 (Vaillant et al., 2008 and data not shown) highlights the need for other markers to identify TICs from established tumors. Increased aldehyde dehydrogenase (ALDH) activity has been found in cancer stem-like populations in multiple cancer types including breast cancer (Ginestier et al., 2007), but its use as a TIC marker in mouse models remains less characterized. We sorted ALDH$^+$ and ALDH$^-$ cells from PyMT tumors (Figure S3I), and found that ALDH$^+$ cells exhibited significantly higher in vitro sphere-forming (Figure 3L) and in vivo tumor-initiating activities (Figures S3J and S3K) compared to ALDH$^-$ cells. Consistent with the ALDH$^+$ population having TIC characteristics, tumors generated by this population recapitulated the phenotypic heterogeneity of the initial tumor, with a similar ratio of ALDH$^+$ and ALDH$^-$ cells (Figure S3L). This indicates that ALDH$^+$ tumor cells are able to self-renew, as well as to differentiate into ALDH$^-$ cells. When MTDH was knocked down in freshly isolated ALDH$^+$ cells from *PyMT;Mtdh*$^{+/+}$ tumors, the sphere-forming activity was significantly reduced (Figure 3M). For MMTV-Wnt tumors, the CD61$^+$ population was demonstrated to possess TIC characteristics and was highly tumorigenic (Vaillant et al., 2008). Consistently, CD61$^+$ tumor cells were capable of generating a greater number of tumor spheres than CD61$^-$ cells (Figure 3N). Importantly, MTDH KD compromised the sphere-forming activities in CD61$^+$ cells from MMTV-Wnt tumors (Figure 3O). These results suggest that MTDH is continuously required for the full functionality of TICs in MTDH-positive tumors.

Protumorigenic Role of MTDH Requires Its Interacting Partner SND1

We previously identified SND1 as the major binding partner of MTDH in human breast cancer cells and it had metastasis-promoting functions similar to MTDH (Blanco et al., 2011). In this study, we found that the interaction between MTDH and SND1 was well conserved in human (Figure S4A) and murine breast cancer cells (Figures S4B–S4D).

To test the necessity of SND1 for the function of MTDH in tumor initiation, we first knocked down SND1 in *PyMT;Mtdh*$^{-/-}$ tumor cells, and rescued the expression of mouse MTDH in these cells (Figure 4A). Reintroduction of MTDH in *PyMT;Mtdh*$^{-/-}$ tumor cells consistently promoted sphere formation in vitro (Figure 4B) and tumor formation in vivo (Figure 4C); however, this effect of MTDH was completely abolished upon SND1 KD (Figures 4B and 4C). If MTDH indeed requires SND1 for its protumorigenic function, we expected knockdown of SND1 in *Mtdh*$^{+/+}$ tumor cells would phenocopy the effect of MTDH deficiency on mammary tumorigenesis. Indeed, SND1 KD in *Mtdh*$^{+/+}$ tumor cells impaired sphere-forming activities in vitro (Figure 4D) and tumor initiation in vivo (Figures 4E and 4F), resembling the effect of MTDH ablation on tumor initiating activities. These results together indicate that MTDH's function on TICs requires the presence of SND1.

To further test whether the physical interaction with SND1 is critical for the function of MTDH, we conducted detailed analysis

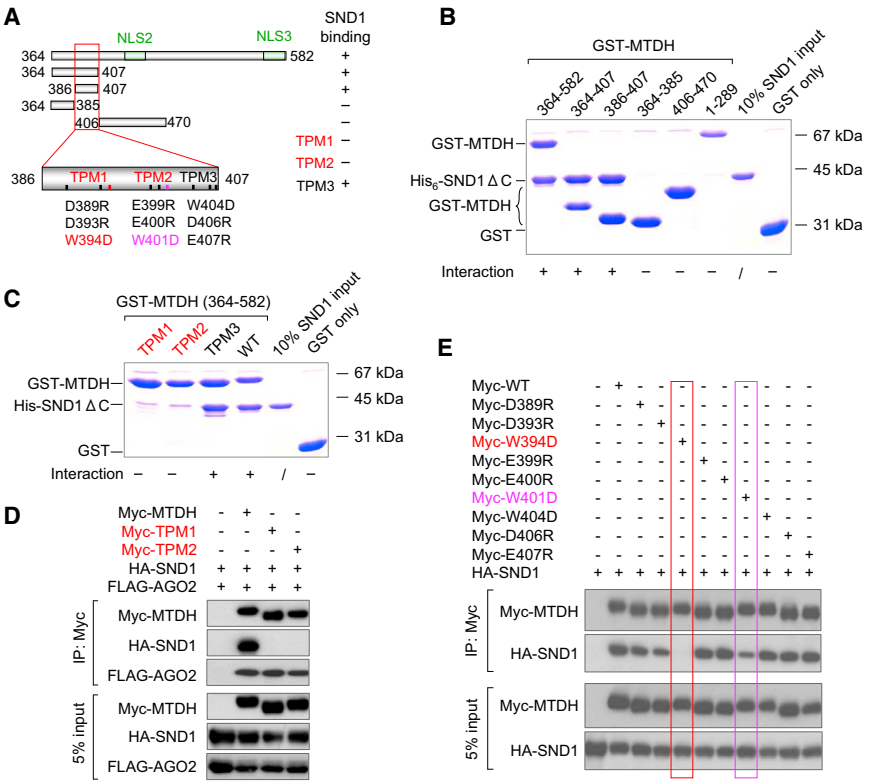

Figure 5. Determination of Key Regions and Residues Mediating the MTDH-SND1 Interaction

(A) Schematics of MTDH fragments and mutants with indicated SND1-binding capability. + indicates binding and – indicates no binding based on results shown below. Two putative nuclear localization signals (432–451 for NLS2 and 561–580 for NLS3) are denoted by green boxes. In the enlarged view of the minimal binding region 386–407, nine residues were targeted for mutagenesis in the current study. Mutations highlighted in red or purple either completely or strongly reduced the binding, respectively.

(B) Pulldown of His6-SND1ΔC by GST-tagged MTDH fragments with indicated boundaries. The bound proteins were examined by SDS-PAGE and depicted with Coomassie blue staining.

(C) Pulldown of His6-SND1ΔC by GST-tagged WT or triple mutant MTDH fragments (364–582). For (B) and (C), one-tenth of the His6-SND1ΔC input is shown, and GST alone was used as a negative control. Representative results of three independent experiments are shown.

(D and E) Lysates from HEK293T cells expressing the indicated ectopic human SND1, AGO2, or MTDH were immunoprecipitated with anti-Myc and immunoblotted with the indicated antibodies.

on the interaction. SND1 contains four N-terminal Staphylococcal nuclease (SN) repeats and a C-terminal Tudor-SN hybrid domain. An SND1 construct missing the C-terminal sequence following the second SN domain (SND1ΔC, 1-339) bound stoichiometrically with MTDH fragment 364–582, but not with MTDH fragment 1–289 (Figures 5A and 5B), resembling the binding behavior of full-length SND1 (Blanco et al., 2011). This allowed us to use the SND1ΔC fragment for the following in vitro binding studies. To map the minimal SND1-binding domain of MTDH, we generated a series of fragments of MTDH within region 364–582 (Figure 5A) and tested their interaction with SND1ΔC. This led to the identification of a 22 amino acid fragment (residues 386–407) sufficient for SND1-binding (Figures 5A and 5B), which was further confirmed by the crystal structure of the MTDH-SND1 complex (manuscript in preparation).

To determine key residues of MTDH that are essential for the interaction, we designed three triple-point mutants (referred to as TPM) with each harboring three amino acid mutations within the 22 amino acid minimal binding domain in the MTDH (364–582) fragment (Figure 5A). In vitro binding assay showed that both TPM1 and TPM2 could not bind SND1ΔC whereas TPM3 bound SND1ΔC as effectively as the WT MTDH (Figure 5C). To examine whether TPM1 and TPM2 interact with SND1 in vivo, full-length HA-tagged SND1 and Myc-tagged MTDH were ectopically expressed in HEK293T cells and the cell lysates were subjected to anti-Myc immunoprecipitation. Consistent with the findings from in vitro binding assays (Figure 5C), HA-SND1 was pulled down with WT but not TPM1 or TPM2 MTDH (Figure 5D). We further analyzed all nine individual mutations using similar strategies and found that W394D completely and W401D partially abolished the binding, whereas other mutations individually did not affect the interaction (Figure 5E). SND1-binding deficient TPM1 and TPM2 MTDH were still able to interact with AGO2 (Figure 5D), another known binding partner of MTDH (Yoo et al., 2011), suggesting that these mutations are unlikely to cause gross conformational changes in MTDH, but rather selectively disrupt the interaction with SND1.

We next tested whether these mutations affect MTDH's function in tumorigenesis. We first stably expressed the murine forms of WT MTDH, TPM1, or TPM2 in *PyMT*;*Mtdh*$^{-/-}$ tumor cells and found that these MTDH mutants lost the ability to interact with SND1 (Figure 6A). Functionally, WT MTDH was able to increase sphere-forming activities of *PyMT;Mtdh*$^{-/-}$ cells in vitro and tumor initiation in vivo, whereas TPM1 or TPM2 mutants failed to do so (Figures 6B–6D). Similar results were observed when the W391D mutant (corresponding to W394D in human MTDH) was tested (Figures 6E–6H). These results strongly suggest that binding residues of MTDH with SND1 are highly conserved in human and mice, and the interaction with SND1 is critical for mediating the functionality of MTDH in regulating TICs activities.

MTDH-Mediated Stabilization of SND1 Confers MECs Survival Advantage under Stress Conditions

SND1 has been reported as a survival factor under various stress conditions (Gao et al., 2010; Sundström et al., 2009; Weissbach and Scadden, 2012). The more prominent role of MTDH in tumor initiation but not normal physiology of mammary glands led us to hypothesize that MTDH, through its interaction with SND1, confers MECs survival advantages under stress conditions during tumorigenesis. Supporting this hypothesis, we detected a significantly higher percentage of apoptotic cells in preneoplastic

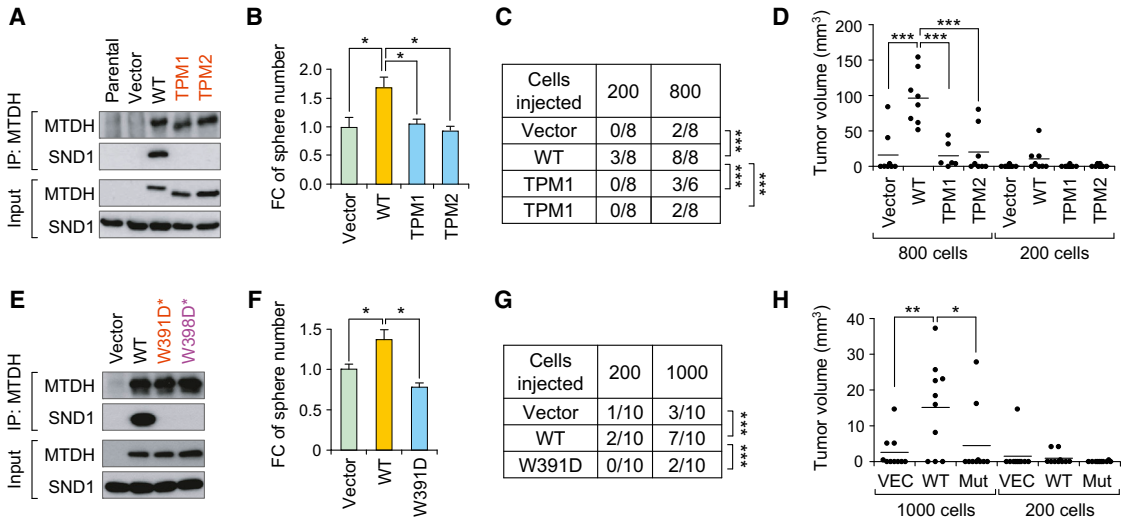

Figure 6. SND1-Binding-Deficient MTDH Fails to Promote Tumor-Initiating Potential of MECs

(A and E) Lysates from PyMT;*Mtdh*$^{-/-}$ MECs reconstituted with vector control, WT or mutant murine MTDH were immunoprecipitated with anti-MTDH antibody and immunoblotted for indicated proteins.

(B and F) Mammosphere assays were performed with PyMT;*Mtdh*$^{-/-}$ pMECs reconstituted with indicated *Mtdh* constructs.

(C, D, G, and H) In vivo tumor formation (C and G for tumor incidence; D and H for tumor volumes) were performed at limiting numbers using PyMT;*Mtdh*$^{-/-}$ pMECs reconstituted with indicated WT or mutant MTDH. *Note: mouse W391D MTDH corresponds to human W394D MTDH; and mouse W398D MTDH corresponds to human W401D MTDH.

Statistics: (B and F) Student's t test. (C and G) Limiting dilution analysis. (D and H) Mann-Whitney test. Data represent mean ± SEM. ***$p < 0.001$, **$p < 0.01$, *$p < 0.05$.

PyMT;Mtdh$^{-/-}$ mammary epithelium than in *PyMT;Mtdh*$^{+/+}$ counterparts, which was not seen in glands without PyMT (Figure 7A). To test the role of MTDH-SND1 interaction under stress conditions in vitro, we treated *PyMT;Mtdh*$^{-/-}$ pMECs, reconstituted with either WT or mutant mouse MTDH, with camptothecin (CPT) to induce DNA replication stress (Figure 7B), a common type of stress during tumor development (Halazonetis et al., 2008). CPT treatment induced apoptosis of MECs in a dosage-dependent manner (Figure 7B). There was a significantly decreased percentage of apoptotic cells in the MTDH-rescued group compared to that in control, and SND1-binding deficient mutations ablated this prosurvival effect of MTDH (Figure 7B).

Consistent with the previous observation that SND1 levels are critical for cell survival under stress conditions, silencing of SND1 in *PyMT;Mtdh*$^{+/+}$ MECs led to a significant increase in apoptosis upon CPT treatment (Figure 7C). Interestingly, we observed a drug dosage-dependent decrease of SND1 protein levels in MECs treated with CPT (Figure 7D). This phenomenon was not unique to this type of stress, as heat shock treatment also resulted in rapid decrease of SND1 (Figure S5). Notably, silencing of MTDH in *PyMT;Mtdh*$^{+/+}$ pMECs accelerated the decrease of SND1 protein (Figure 7D). Conversely, restoration of WT, but not SND1-binding deficient MTDH, in *PyMT;Mtdh*$^{-/-}$ MECs stabilized SND1 protein under these stress conditions (Figures 7E and S5). Thus, these data collectively suggest that MTDH promotes survival under stress conditions by interacting with and stabilizing survival factor SND1.

To provide a better understanding of how SND1 exerts its prosurvival function, we performed transcriptomic profiling of control versus SND1-KD *PyMT;Mtdh*$^{+/+}$ pMECs under CPT treatment (Figures 7F–7H). Ingenuity Pathway Analysis revealed that genes upregulated by SND1 (Figure 7F, > 2-fold change, $p < 0.05$) showed a significant enrichment for molecular and cellular functions including "cell death and survival," "cell cycle," and "DNA repair" (Figure 7G), processes related to CPT-induced replication stress. Notably, a significant portion of SND1-upregulated genes were implicated in the "cell death and survival" category and the expression of these genes collectively was predicted to significantly activate cell viability function (Figure 7H, red) and compromise cell death and apoptosis (Figure 7H, green). Therefore, the ability of SND1 to globally activate prosurvival genes may underlie its role in protecting cells from stress-induced cell death (Figure 7C). To substantiate the hypothesis that MTDH regulates survival through interacting with and stabilizing SND1, we profiled *PyMT;Mtdh*$^{-/-}$ pMECs reconstituted with either WT or SND1-binding deficient mutant mouse MTDH (W391D). Gene set enrichment analysis demonstrated that SND1-upregulated gene signature was significantly enriched in *PyMT;Mtdh*$^{-/-}$ pMECs reconstitured with WT versus mutant MTDH (Figure 7I).

MTDH and SND1 Are Important for Tumor-Initiating Activities of Human Breast Cancer Cells

To demonstrate the important roles of both MTDH and SND1 in tumor-initiating activities in human breast cancer, we silenced MTDH or SND1 in multiple human breast cancer models, including: (1) HER2/Neu-transformed human breast epithelial cells (HMLE-N; Mani et al., 2008; Figures 8A, 8B, S6A, and S6B), (2) human primary patient-derived xenografts (DeRose et al., 2011; Zhang et al., 2013b; Figures 8C, 8D, S6C, and S6D; data not shown), and (3) the MDA-MB-231 human breast cancer cell line (Figures 8E–8H). Knockdown of either MTDH or

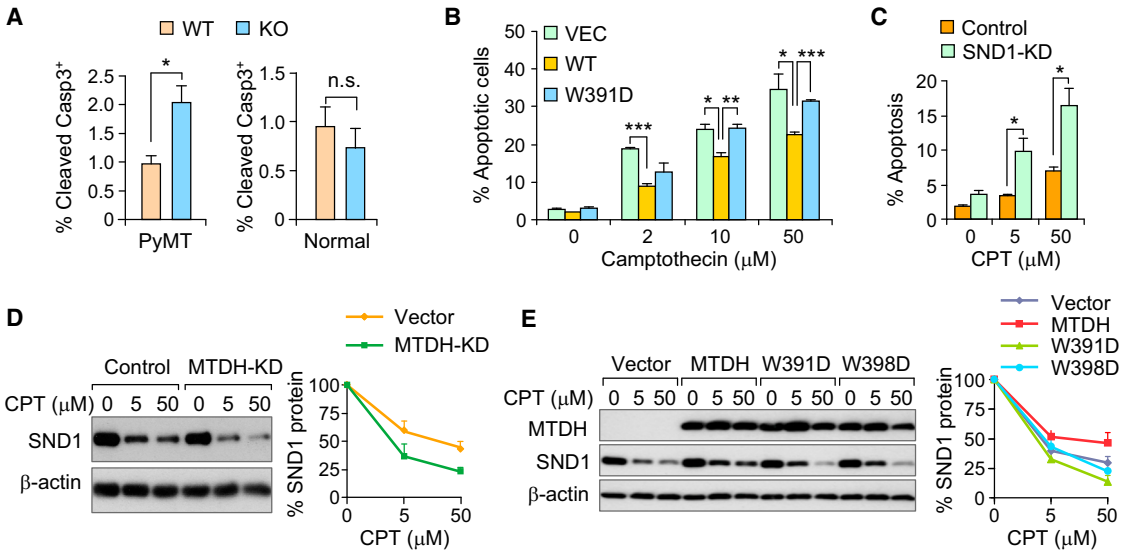

G

Molecular and cellular functions	p value	# of molecules
Cell death and survival	6.77E-08 – 1.27E-02	137
Cell cycle	9.59E-23 – 1.25E-02	111
Cellular assembly and organization	9.59E-23 – 1.25E-02	94
DNA replication, recombination, and repair	9.59E-23 – 1.29E-02	89
Cellular movement	2.26E-09 – 1.29E-02	33

H

Functional annotation	p value	Predicted activation state	Activation z-score
Cell survival	6.51E-04	Increased	5.253
Cell viability	2.62E-03	Increased	4.834
Cell viability of tumor cell lines	3.79E-03	Increased	2.984
Cell viability of myeloma cell lines	2.87E-05	Increased	2.345
Cell viability of cancer cells	6.49E-03	Increased	2.236
Cell viability of embryonic cell lines	1.95E-05	Increased	2.138
Apoptosis	6.77E-08		-1.496
Cell death	9.97E-07		-1.59

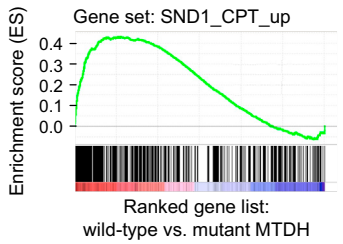

Figure 7. MTDH Confers Survival Advantage by Interacting with and Stabilizing Pro-Survival Protein SND1 under Stress

(A) Quantification of cleaved caspase 3-positive MECs from normal or MMTV-PyMT preneoplastic glands (n > 3) of WT or KO females.

(B) The effect of CPT on the apoptosis of *PyMT;Mtdh*$^{-/-}$ pMECs reconstituted with indicated *Mtdh* constructs was determined by PI and Hoechst staining.

(C) The effect of CPT on the apoptosis of control or SND1-KD *PyMT;Mtdh*$^{+/+}$ pMECs.

(D) Protein levels of SND1 and β-actin (loading control) in control or MTDH-KD *PyMT;Mtdh*$^{+/+}$ pMECs treated with CPT at indicated concentrations for 36 hr. Degradation curve (right) represents the average of three independent experiments.

(E) Western blotting of SND1, MTDH, and β-actin (loading control) in *PyMT;Mtdh*$^{-/-}$ MECs reconstituted with indicated constructs after CPT treatment for 48 hr. Degradation curves (right) represent average of three independent experiments.

(F) Heat map representation of microarray data displaying the expression of SND1-upregualted genes (n = 504, fold change > 2, $p < 0.05$) in control versus SND1-KD *PyMT;Mtdh*$^{+/+}$ pMECs under CPT (50 μM) treatment for 36 hr. Color key indicates log2 values.

(G) Ingenuity pathway analysis shows the top five molecular and cellular functions of SND1-upregulated genes shown in (F) and the number of molecules/genes implicated in each category.

(H) Effects of SND1-upregulated genes in cell survival and cell death functions. Z scores were calculated based on gene expression changes and gene functions as specified by the ingenuity knowledge base. A given function is predicted to be significantly increased when $z > 2$ or decreased when $z < -2$.

(I) Gene set enrichment analysis plot showing the enrichment of SND1-upregulated gene signature in *PyMT;Mtdh*$^{-/-}$ MECs rescued with mouse WT MTDH as compared to those rescued with W391D mutant MTDH. All cells were treated with CPT (50 μM). NES, normalized enrichment score.

Statistics: (A–C) Student's t test. Data represent mean ± SEM. ***$p < 0.001$, **$p < 0.01$, *$p < 0.05$. See also Figure S5.

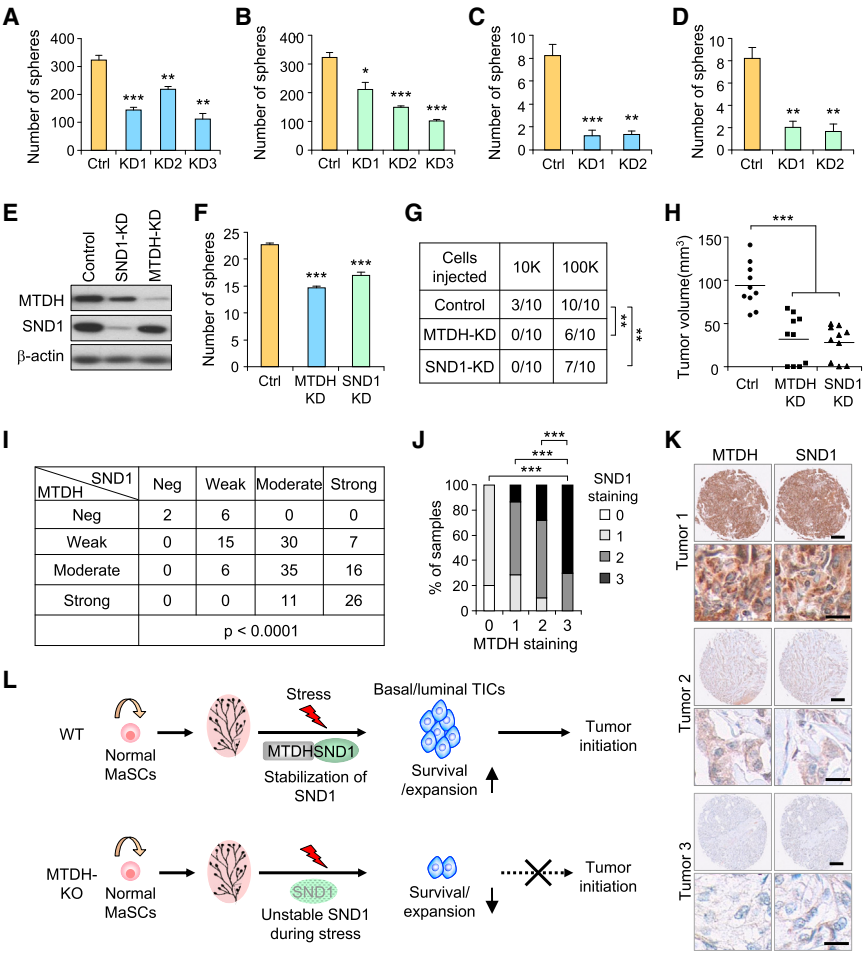

Figure 8. MTDH and SND1 Are Important for In Vitro Sphere-Forming and In Vivo Tumor-Initiating Activities of Human Breast Cancer Cells

(A and B) MTDH (A) or SND1 (B) was knocked down in HMLE-Neu cells and tumorsphere assays were performed in triplicate.

(C and D) MTDH (C) or SND1 (D) was knocked down in the BCM-4013 patient-derived xenografted (PDX) tumor cells and tumorsphere assays were performed in triplicate.

(E) MTDH or SND1 was knocked down in MDA-MB-231 cells, and the KD efficiency was measured by immunoblotting.

(F) Tumorsphere assays of MDA-MB-231 cells were performed in triplicate.

(G and H) Tumor incidence (G) and volumes (H) 5 weeks after injection of limiting numbers of MDA-MB-231 cells.

(I) The protein levels of MTDH and SND1 in human invasive mammary carcinomas (n = 154) were determined by IHC staining of a breast cancer tissue microarray (BR1921a, US Biomax). The staining intensity in tumor cells was scored as 0 (negative), 1 (weak), 2 (moderate), or 3 (strong).

(J) Bar graph presentation of (I).

(K) Representative tumor specimens with strong (tumor 1), weak (tumor 2), and negative (tumor 3) staining of MTDH and SND1. Scale bar represents 200 μm (top) and 20 μm (bottom) for each tumor.

(L) Schematic illustration depicting the essential role of MTDH in tumor initiation but not normal gland development. Under stress conditions during tumorigenesis, the MTDH-SND1 interaction protects SND1 from stress-induced degradation and supports the survival and activities of both basal and luminal TICs.

Statistics: (A–D and F) Student's t test. (G) Limiting dilution analysis. (H) Mann-Whitney test. (I and J) Chi-square test. Data represent mean ± SEM. ***p < 0.001, **p < 0.01, *p < 0.05. See also Figure S6.

SND1 significantly reduced in vitro tumorsphere formation of all models tested and tumor initiation of MDA-MB-231 cells in vivo.

We further examined whether MTDH-mediated stabilization of SND1 occurs in human breast cancer samples. We stained a human breast cancer tissue microarray (TMA) with antibodies against MTDH and SND1 (Figures 8I-8K), after confirming the specificity of the antibodies (Figures S6E and S6F). We found a positive correlation between staining scores of MTDH and SND1 (Figures 8I and 8J), which was confirmed using an independent TMA (Figures S6G and S6H). Of note, *MTDH* and *SND1* were not correlated at the mRNA levels (Figure S6I). These data support a key role of MTDH in posttranscriptional regulation of SND1 in breast cancer, consistent with our findings that MTDH interacts with and stabilizes SND1 under stress conditions during tumorigenesis.

To further explore the clinical importance of the MTDH-SND1 interaction, we analyzed the NKI295 human breast cancer microarray data set (van de Vijver et al., 2002). We stratified patients into four different groups based on median expression for both *SND1* and *MTDH*. Primary tumors with high mRNA levels of both *MTDH* and *SND1* were significantly larger (Figure S6J), less differentiated (Figure S6K), and correlated with a shorter distant metastasis-free survival (Figure S6L), supporting a functional cooperation between MTDH and SND1 in human breast cancer in tumor development, metastasis, and recurrence. Consistent with its tumor-promoting function in diverse mammary tumor models, we further found that higher levels of *MTDH* predicted poor prognosis across multiple breast cancer subtypes in the KM-plotter data set (Figure S6M). The seemingly stronger prognostic power of *MTDH* in luminal A subtype is likely due to a significantly larger sample size in this group compared to other subtypes.

DISCUSSION

Whereas the classical clonal evolution theory of tumor progression postulates that metastatic capabilities are endowed by random genetic changes occurring in rare cells within the primary tumor, genomic and clinical studies paradoxically demonstrate that the likelihood to metastasize can be predicted by profiling the bulk of primary tumors (van de Vijver et al., 2002). This suggests metastatic potential may be conferred by

oncogenic events that possess additional metastasis-promoting functions (Bernards and Weinberg, 2002), and therefore these genetic changes can occur and be selected early in tumor evolution (Vanharanta and Massagué, 2013). Supporting this notion, several metastasis-promoting genes have been shown to promote primary tumor growth in xenograft models (Vanharanta and Massagué, 2013; Wan et al., 2013). The recurrent amplification/overexpression of *MTDH* in human primary breast tumors may therefore implicate MTDH in tumorigenesis in addition to its reported role in promoting breast cancer metastasis. Whereas previous studies using human or murine breast cancer cell lines failed to reveal any effect of MTDH on primary tumor formation in xenograft models (Brown and Ruoslahti, 2004; Hu et al., 2009), genetically engineered mouse models used in this study enabled us to uncover a role of MTDH in regulating the expansion and activities of TICs at early stages of tumorigenesis, thus establishing another molecular link between primary tumor initiation with the acquisition of metastatic traits. This effect of MTDH on tumor initiation has likely been masked when a large number of highly aggressive and late-stage tumor cells were used in previous xenograft studies. Consistent with this speculation, when late-stage PyMT tumor cells were transplanted in large quantities, we failed to observe a difference in tumor initiation between *Mtdh* WT and KO cells (data not shown). Nevertheless, TICs from MTDH-positive established mammary tumors, such as $ALDH^+$ cells and $CD61^+$ cells from PyMT and Wnt-induced tumors, respectively, remain sensitive to MTDH inhibition, suggesting that MTDH-dependent mechanisms are at play in established tumors to maintain the optimal functionality of TICs, and therefore blocking MTDH and its regulated pathways will be beneficial to cancer patients with aberrant expression of MTDH.

It has been suggested that initiating genetic lesions exert a significant influence on the histopathology and molecular features of mammary tumors from both humans and transgenic animals. For example, Wnt signaling induces mammary tumors with features resembling more primitive progenitor cells as compared to PyMT and ErbB2 (Li et al., 2003). Remarkably, we found that MTDH is required for the functionality of TICs across these different tumor models. Consistently, MTDH expression does not significantly correlate with specific subtypes of human breast cancer (Hu et al., 2009) and higher levels of MTDH predict poor prognosis across different subtypes. These results together corroborate the idea that MTDH promotes tumor initiation in an oncogene- and lineage-independent manner, in contrast to lineage-specific tumor-promoting genes, such as luminal tumor survival factor PDEF (Buchwalter et al., 2013). The broad function of MTDH in tumorigenesis is also in agreement with its frequent upregulation in a diverse spectrum of cancer types (Emdad et al., 2013; Wan and Kang, 2013).

Tumors formed in the absence of MTDH exhibited similar histological features as MTDH-positive tumors, suggesting that MTDH may not alter the cell of origin or cell fate of TICs, but instead influence their tumorigenic potential. This, together with the observation that *Mtdh* KO had little effect on the activities of MaSCs, establish MTDH as a critical regulator of TICs that is distinct from other cell fate regulators, such as Wnt signaling (Lento et al., 2013), Slug/Sox9 (Guo et al., 2012), and GATA3 (Kouros-Mehr et al., 2008), which regulate tumorigenesis by virtue of their abilities to mediate the conversion between differentiated cells and more primitive stem/progenitor cells in both normal and malignant contexts.

We and others have identified SND1 as a major binding partner of MTDH (Blanco et al., 2011; Meng et al., 2012; Yoo et al., 2011). However, a discrepancy exists regarding the binding domains of MTDH with SND1, because two nonoverlapping regions of MTDH, namely amino acids 364–470 (Blanco et al., 2011) and 101–205 (Yoo et al., 2011), were each independently mapped as the only essential domain mediating MTDH's interaction with SND1. Our study further determines a minimal fragment of MTDH (386–407) sufficient for the interaction and identifies two key residues within this fragment critical for the interaction. These findings enabled us to demonstrate that the interaction with SND1 is pivotal for the function of MTDH. These findings also establish SND1 as a critical regulator of mammary TICs. Importantly, the interaction between MTDH and SND1 as well as the binding residues are well conserved between human and mice, highlighting the possibility that our findings in mouse models may be highly relevant to human cancer, as suggested by the current functional and clinical analyses.

Tumorigenesis is accompanied by diverse stresses that tumor cells have to overcome, including oncogene-induced DNA replication/damage stress. We demonstrated that SND1 is required for the expression of a cohort of prosurvival genes in cells under stress conditions, and silencing of SND1 sensitizes transformed MECs to replication stress-induced apoptosis. These results are consistent with previous reports that established SND1 as a prosurvival protein under various stress conditions (Gao et al., 2010; Sundström et al., 2009; Weissbach and Scadden, 2012). Furthermore, the physical interaction with MTDH is essential to protect SND1 from degradation and sustain SND1-regulated gene signature under stress conditions. It is thus possible that MTDH protects TICs from attritions under stress conditions during tumorigenesis, at least in part, by virtue of its ability to interact with and stabilize SND1 (Figure 8L). It remains unclear how SND1 regulates downstream prosurvival genes. SND1 is a multifunctional protein that has been reported to be involved in several gene regulatory processes, including transcriptional control, mRNA splicing, RNA stress granule formation, and RNA-induced silencing complex (RISC) machinery (reviewed in Wan and Kang, 2013). Future studies are warranted to investigate how SND1 modulates gene expression in response to stress conditions to promote cellular survival.

In addition to providing a molecular link between tumor initiation and metastatic capabilities, our findings suggest several lines of potential translational applications. First, the functional importance of MTDH and SND1 in sustaining TIC function, if extensively validated in patient-derived tumor grafts, may establish these proteins as potential therapeutic targets in cancer treatment. In addition, our results on the MTDH-SND1 interaction may facilitate the screening or design of small molecule inhibitors that can disrupt the interaction of MTDH and SND1. Our results also highlight the tumor-specific requirement of MTDH and suggest that systemic targeting of the MTDH-SND1 module may be well tolerated by cancer patients, as whole organism knockout of *Mtdh* does not cause significant defects in mice. Future studies are needed to fully assess the therapeutic

potential of targeting the MTDH-SND1 interaction in cancer progression.

EXPERIMENTAL PROCEDURES

Mice

All experimental protocols involving mice were approved by Institutional Animal Care and Use Committee of Princeton University. *Mtdh*-KO mice were generated by injecting ES cell line XB780 (BayGenomics) into the C57BL/6 blastocysts followed by confirmation of germline transmission. KO mice were then backcrossed to FVB background for more than six generations before breeding with MMTV-PyMT, MMTV-ErbB2, MMTV-Wnt transgenic mice (Jackson Laboratory) in FVB background. To create the *MMTV-Mtdh* construct, the mouse *Mtdh* coding sequence was inserted into the pMMTV-SV40 vector, then the expression cassette was linearized and microinjected into the pronuclei of zygotes from FVB mice. For spontaneous tumorigenesis studies, female mice carrying the specific oncogenes were examined weekly for mammary tumors. Tumors were considered established when they became palpable for 2 consecutive weeks, and tumors were measured by calipers for calculation of tumor volumes ($\pi \times \text{length} \times \text{width}^2/6$). Lung nodules were counted directly after fixation (MMTV-PyMT models) or after sectioning and staining of the lungs (MMTV-ErbB2 model).

Human Breast Cancer TMAs

Two human breast TMAs were used in the study to examine the correlation of MTDH and SND1 protein levels. One TMA was purchased from US Biomax (BR1921a) and a second TMA was obtained from the Cancer Institute of New Jersey (YMTA_201). Both sets of TMAs used de-identified tumor samples and were considered exempt by the Institutional Review Boards of Princeton University and the Rutgers New Jersey Medical School.

Harvesting Mammary Epithelial Cells and Flow Cytometry

Single cell suspensions of mammary glands or tumors were prepared as previously described (Shackleton et al., 2006). Briefly, tissues were dissected, minced into small pieces and digested for 1 hr at 37°C in culture medium (1:1 Dulbecco's modified Eagle's medium [DMEM]: Ham's F-12 medium containing 5% FBS, 10 ng/ml epidermal growth factor [EGF], 500 ng/ml hydrocortisone, 5 μg/ml insulin, 20 ng/ml cholera toxin, and 1% Pen/Strep) supplemented with 300 U/ml type 1A collagenase (Sigma) and 100 U/ml hyaluronidase (Sigma). Organoids were sequentially suspended with 0.25% trypsin-EDTA for 1.5 min, 5 mg/ml Dispase (Invitrogen), and 0.1 mg/ml DNase (Sigma) for 5 min, and 0.64% ammonium chloride for 5 min at 37°C before filtration through a 40 μm nylon cell strainer and antibody staining. Mammary epithelial cells were incubated with an antibody cocktail containing CD31, CD45, TER119, CD24, CD29, and CD61 for 30 min followed by secondary antibody staining for 20 min before FACS analysis or sorting.

Limiting Dilution Assays

For mammary gland reconstitution assays, single cell suspensions of MECs from mammary glands of 7- or 8-week-old female mice were sorted and injected into cleared mammary fat pads of 3-week-old recipient mice. The outgrowths were analyzed at 6–8 weeks after transplantation. For tumorigenesis assays, single cell suspensions of primary MECs were transplanted into FVB WT recipient mice unless otherwise indicated.

Mammosphere/Tumorsphere Assays

Single cells were plated in ultralow attachment plates (Corning) with sphere media (1:1 DMEM: Ham's 12 supplemented with B27 [Invitrogen], 20 ng/ml EGF [Novoprotein], 20 ng/ml basic fibroblast growth factor, and 4 μg/ml heparin). Spheres were counted 4–7 days after plating.

Microarray Analysis

RNA was extracted from indicated tumor cells under CPT (50 μM) treatment and analyzed with Agilent Whole Mouse Genome 4 × 44k arrays. RNA samples were labeled with Cy5 using the Agilent Low RNA Input Linear Amplification Kit and hybridized along with the Cy3-labeled Mouse Universal Reference RNA (Stratagene). Arrays were scanned with an Agilent G2565BA scanner and analyzed with the Agilent Feature Extraction v9.5 software. The Cy5/Cy3 ratios were calculated using the feature medium signal and normalized by the array median. Genes with > 2-fold (average) changes and Student's t test p values < 0.05 were included as SND1-regulated genes.

Statistical Analysis

All results wherever necessary were subjected to statistical analysis. A log-rank test, a nonparametric Mann-Whitney test, Chi-square test, and unpaired, two-sided, independent Student's t test with equal variance assumption were used for most studies as indicated in the figure legends. For limiting dilution assay, the frequency of MaSCs or TICs and statistics were calculated using L-calc software (StemCell Technologies). The p values were denoted as $^*p < 0.05$, $^{**}p < 0.01$, and $^{***}p < 0.001$ in all figures.

ACCESSION NUMBERS

The Gene Expression Ominibus accession number for all raw microarray data files is GSE55522.

SUPPLEMENTAL INFORMATION

Supplemental Information includes Supplemental Experimental Procedures and six figures and can be found with this article online at http://dx.doi.org/10.1016/j.ccr.2014.04.027.

ACKNOWLEDGMENTS

We thank J.T. Eggenschwiler, J. Levorse, and M. Bhaumik for helping with the generation of *Mtdh*-knockout and *MMTV-Mtdh* transgenic mice, R.A. Weinberg for the HMLE-N cell line, A.L. Welm and M.T. Lewis for the human breast cancer PDX lines, K. Pantel and H. Wikman for providing human breast TMAs, W. Muller for the pMMTV-SV40 plasmid, X.H. Zhang for bioinformatic analysis, C. DeCoste for assistance with flow cytometry, and L. Cong, W. Chen for IHC analysis. The work was supported by a Charlotte Elizabeth Procter Fellowship to L.W. and grants from the Department of Defense (BC123187), Brewster Foundation, Komen for the Cure, and the NIH (R01CA134519) to Y.K. and a grant from Breast Cancer Research foundation to B.G.H. This research was also supported by the Transgenic/Knockout, Tissue Analytic Service and Flow Cytometry Shared Resources of the Cancer Institute of New Jersey (P30CA072720).

Received: November 1, 2013
Revised: March 5, 2014
Accepted: April 30, 2014
Published: June 26, 2014

REFERENCES

Asselin-Labat, M.L., Sutherland, K.D., Barker, H., Thomas, R., Shackleton, M., Forrest, N.C., Hartley, L., Robb, L., Grosveld, F.G., van der Wees, J., et al. (2007). Gata-3 is an essential regulator of mammary-gland morphogenesis and luminal-cell differentiation. Nat. Cell Biol. *9*, 201–209.

Bernards, R., and Weinberg, R.A. (2002). A progression puzzle. Nature *418*, 823.

Blanco, M.A., Alečković, M., Hua, Y., Li, T., Wei, Y., Xu, Z., Cristea, I.M., and Kang, Y. (2011). Identification of staphylococcal nuclease domain-containing 1 (SND1) as a Metadherin-interacting protein with metastasis-promoting functions. J. Biol. Chem. *286*, 19982–19992.

Brown, D.M., and Ruoslahti, E. (2004). Metadherin, a cell surface protein in breast tumors that mediates lung metastasis. Cancer Cell *5*, 365–374.

Buchwalter, G., Hickey, M.M., Cromer, A., Selfors, L.M., Gunawardane, R.N., Frishman, J., Jeselsohn, R., Lim, E., Chi, D., Fu, X., et al. (2013). PDEF promotes luminal differentiation and acts as a survival factor for ER-positive breast cancer cells. Cancer Cell *23*, 753–767.

DeRose, Y.S., Wang, G., Lin, Y.C., Bernard, P.S., Buys, S.S., Ebbert, M.T., Factor, R., Matsen, C., Milash, B.A., Nelson, E., et al. (2011). Tumor grafts

derived from women with breast cancer authentically reflect tumor pathology, growth, metastasis and disease outcomes. Nat. Med. *17*, 1514–1520.

Emdad, L., Das, S.K., Dasgupta, S., Hu, B., Sarkar, D., and Fisher, P.B. (2013). AEG-1/MTDH/LYRIC: signaling pathways, downstream genes, interacting proteins, and regulation of tumor angiogenesis. Adv. Cancer Res. *120*, 75–111.

Gao, X., Ge, L., Shao, J., Su, C., Zhao, H., Saarikettu, J., Yao, X., Yao, Z., Silvennoinen, O., and Yang, J. (2010). Tudor-SN interacts with and co-localizes with G3BP in stress granules under stress conditions. FEBS Lett. *584*, 3525–3532.

Ginestier, C., Hur, M.H., Charafe-Jauffret, E., Monville, F., Dutcher, J., Brown, M., Jacquemier, J., Viens, P., Kleer, C.G., Liu, S., et al. (2007). ALDH1 is a marker of normal and malignant human mammary stem cells and a predictor of poor clinical outcome. Cell Stem Cell *1*, 555–567.

Guo, W., Keckesova, Z., Donaher, J.L., Shibue, T., Tischler, V., Reinhardt, F., Itzkovitz, S., Noske, A., Zürrer-Härdi, U., Bell, G., et al. (2012). Slug and Sox9 cooperatively determine the mammary stem cell state. Cell *148*, 1015–1028.

Halazonetis, T.D., Gorgoulis, V.G., and Bartek, J. (2008). An oncogene-induced DNA damage model for cancer development. Science *319*, 1352–1355.

Herschkowitz, J.I., Simin, K., Weigman, V.J., Mikaelian, I., Usary, J., Hu, Z., Rasmussen, K.E., Jones, L.P., Assefnia, S., Chandrasekharan, S., et al. (2007). Identification of conserved gene expression features between murine mammary carcinoma models and human breast tumors. Genome Biol. *8*, R76.

Hu, G., Chong, R.A., Yang, Q., Wei, Y., Blanco, M.A., Li, F., Reiss, M., Au, J.L., Haffty, B.G., and Kang, Y. (2009). MTDH activation by 8q22 genomic gain promotes chemoresistance and metastasis of poor-prognosis breast cancer. Cancer Cell *15*, 9–20.

Kouros-Mehr, H., Bechis, S.K., Slorach, E.M., Littlepage, L.E., Egeblad, M., Ewald, A.J., Pai, S.Y., Ho, I.C., and Werb, Z. (2008). GATA-3 links tumor differentiation and dissemination in a luminal breast cancer model. Cancer Cell *13*, 141–152.

Lento, W., Congdon, K., Voermans, C., Kritzik, M., and Reya, T. (2013). Wnt signaling in normal and malignant hematopoiesis. Cold Spring Harb. Perspect. Biol. *5*, 5.

Li, Y., Welm, B., Podsypanina, K., Huang, S., Chamorro, M., Zhang, X., Rowlands, T., Egeblad, M., Cowin, P., Werb, Z., et al. (2003). Evidence that transgenes encoding components of the Wnt signaling pathway preferentially induce mammary cancers from progenitor cells. Proc. Natl. Acad. Sci. USA *100*, 15853–15858.

Mani, S.A., Guo, W., Liao, M.J., Eaton, E.N., Ayyanan, A., Zhou, A.Y., Brooks, M., Reinhard, F., Zhang, C.C., Shipitsin, M., et al. (2008). The epithelial-mesenchymal transition generates cells with properties of stem cells. Cell *133*, 704–715.

Meng, X., Zhu, D., Yang, S., Wang, X., Xiong, Z., Zhang, Y., Brachova, P., and Leslie, K.K. (2012). Cytoplasmic Metadherin (MTDH) provides survival advantage under conditions of stress by acting as RNA-binding protein. J. Biol. Chem. *287*, 4485–4491.

Perou, C.M., Sørlie, T., Eisen, M.B., van de Rijn, M., Jeffrey, S.S., Rees, C.A., Pollack, J.R., Ross, D.T., Johnsen, H., Akslen, L.A., et al. (2000). Molecular portraits of human breast tumours. Nature *406*, 747–752.

Shackleton, M., Vaillant, F., Simpson, K.J., Stingl, J., Smyth, G.K., Asselin-Labat, M.L., Wu, L., Lindeman, G.J., and Visvader, J.E. (2006). Generation of a functional mammary gland from a single stem cell. Nature *439*, 84–88.

Sundström, J.F., Vaculova, A., Smertenko, A.P., Savenkov, E.I., Golovko, A., Minina, E., Tiwari, B.S., Rodriguez-Nieto, S., Zamyatnin, A.A., Jr., Välineva, T., et al. (2009). Tudor staphylococcal nuclease is an evolutionarily conserved component of the programmed cell death degradome. Nat. Cell Biol. *11*, 1347–1354.

Vaillant, F., Asselin-Labat, M.L., Shackleton, M., Forrest, N.C., Lindeman, G.J., and Visvader, J.E. (2008). The mammary progenitor marker CD61/beta3 integrin identifies cancer stem cells in mouse models of mammary tumorigenesis. Cancer Res. *68*, 7711–7717.

van de Vijver, M.J., He, Y.D., van't Veer, L.J., Dai, H., Hart, A.A., Voskuil, D.W., Schreiber, G.J., Peterse, J.L., Roberts, C., Marton, M.J., et al. (2002). A gene-expression signature as a predictor of survival in breast cancer. N. Engl. J. Med. *347*, 1999–2009.

Vanharanta, S., and Massagué, J. (2013). Origins of metastatic traits. Cancer Cell *24*, 410–421.

Wan, L., and Kang, Y. (2013). Pleiotropic roles of AEG-1/MTDH/LYRIC in breast cancer. Adv. Cancer Res. *120*, 113–134.

Wan, L., Pantel, K., and Kang, Y. (2013). Tumor metastasis: moving new biological insights into the clinic. Nat. Med. *19*, 1450–1464.

Weissbach, R., and Scadden, A.D. (2012). Tudor-SN and ADAR1 are components of cytoplasmic stress granules. RNA *18*, 462–471.

Yin, Y., Bai, R., Russell, R.G., Beildeck, M.E., Xie, Z., Kopelovich, L., and Glazer, R.I. (2005). Characterization of medroxyprogesterone and DMBA-induced multilineage mammary tumors by gene expression profiling. Mol. Carcinog. *44*, 42–50.

Yoo, B.K., Santhekadur, P.K., Gredler, R., Chen, D., Emdad, L., Bhutia, S., Pannell, L., Fisher, P.B., and Sarkar, D. (2011). Increased RNA-induced silencing complex (RISC) activity contributes to hepatocellular carcinoma. Hepatology *53*, 1538–1548.

Zhang, W., Tan, W., Wu, X., Poustovoitov, M., Strasner, A., Li, W., Borcherding, N., Ghassemian, M., and Karin, M. (2013a). A NIK-IKKα module expands ErbB2-induced tumor-initiating cells by stimulating nuclear export of p27/Kip1. Cancer Cell *23*, 647–659.

Zhang, X., Claerhout, S., Prat, A., Dobrolecki, L.E., Petrovic, I., Lai, Q., Landis, M.D., Wiechmann, L., Schiff, R., Giuliano, M., et al. (2013b). A renewable tissue resource of phenotypically stable, biologically and ethnically diverse, patient-derived human breast cancer xenograft models. Cancer Res. *73*, 4885–4897.